Spatial correlations in a finite-range Kuramoto model

Sebastian Wüster[1,*] and Rajasekaran Bhavna[2]
[1]*Department of Physics, Indian Institute of Science Education and Research, Bhopal, Madhya Pradesh 462 023, India*
[2]*Department of Biological Sciences, Tata Institute of Fundamental Research, 400005 Mumbai, India*

(Received 19 November 2019; accepted 21 April 2020; published 15 May 2020)

We study spatial correlations between oscillator phases in the steady state of a Kuramoto model, in which phase oscillators that are randomly distributed in space interact with constant strength but within a limited range. Such a model could be relevant, for example, in the synchronization of gene expression oscillations in cells, where only oscillations of neighboring cells are coupled through cell-cell contacts. We analytically infer spatial phase-phase correlation functions from the known steady-state distribution of oscillators for the case of homogenous frequencies and show that these can contain information about the range and strength of interactions, provided the noise in the system can be estimated. We suggest a method for the latter, and also explore when correlations appear to be ergodic in this model, which would enable an experimental measurement of correlation functions to utilize temporal averages. Simulations show that our techniques also give qualitative results for the model with heterogenous frequencies. We illustrate our results by comparison with experimental data on genetic oscillations in the segmentation clock of zebrafish embryos.

DOI: 10.1103/PhysRevE.101.052210

I. INTRODUCTION

The Kuramoto model [1–3] is paradigmatic for the study of synchronization [4]. It has been applied in a diverse range of settings, such as neuronal activity [5], coupled magnetic spin torque oscillators [6], coupled Josephson junction arrays [7,8], atomic lasing [9], and flashing fireflies [10]. Also during vertebrate development, genetic oscillations in a mechanism called the segmentation clock are synchronized to generate a rhythmic pattern with a temporal periodicity that is converted into a striped spatial pattern of gene expression that makes up the embryonic segments across vertebrates [11–14].

Despite the conceptual simplicity of the basic Kuramoto model, containing only a set of phase oscillators coupled via a phase synchronizing interaction that is identical for all oscillator pairs, the presence of noise already gives rise to a host of additional mathematical features such as pattern formation, bistability, and bifurcations [3,15,16]. Extensions of the model additionally consider range-dependent couplings [17,18] or time-delayed coupling [19], further enriching the phenomenology.

Here we study phase correlations in a specific variant of the model, with a finite-interaction range such that only oscillators that are spatially separated by less than R_0 interact with constant instantaneous coupling strength κ_0, while subjected to noise [20,21]. Our objective is to contribute to experimental estimates of oscillator coupling strengths leading to synchronization in the segmentation clock [11–14,22–24] of the developing zebrafish embryos, but the results are more generally applicable.

We demonstrate that in the case of homogenous frequencies, where all oscillators share the same natural frequency, the essential parameters of our interaction model, the range R_0 and coupling strength κ_0, can be directly inferred from nonlocal phase correlations in weakly synchronized regimes. They can still be constrained through fitting the model to data in more strongly synchronized regimes, or for heterogeneous frequencies. We follow up on earlier studies on parameter reconstruction in a similar model [25], while significantly extending these results for cases with unknown or mobile oscillator positions, unknown network connectivity, and finite-range interactions.

We finally explore correlations in the context of data from genetic oscillators of the segmentation clock within developing zebrafish embryos. The oscillating quantity is the level of gene expression within a cell. These cells characteristically behave as autonomous cellular oscillators, while synchronizing interactions are provided by the intercellular delta-notch coupling [26]. Parameters for models describing the coupled cell system, such as coupling strength, cell-autonomous period, and the coupling delays, have been inferred by disruption of delta-notch intercellular coupling under various genetic conditions [27,28] and the range of such interactions has been theoretically estimated in another study [29]. Recently, single-cell-based phase oscillator measurements provided a framework to constrain the interaction parameters [23].

Since, within a biological context, individual systems are typically insufficiently reproducible to allow a thorough ensemble average, an interesting question is to what extent the model used here is ergodic and hence allows the inference of ensemble averages by replacing them with a time average in a single system. We investigate this question numerically, and find that in some cases of interest to us, the model behaves ergodically.

This article is organized as follows: In Sec. II we describe the version of Kuramoto (or Kuramoto-Sakaguchi) model that we study and its known steady-state solution [25], which

*sebastian@iiserb.ac.in

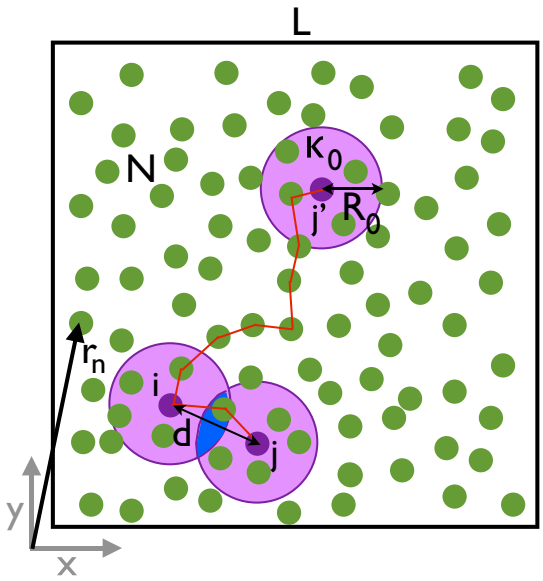

FIG. 1. Assembly of N phase oscillators (small green circles) spread in 2D over a square of side-length L. Each oscillator interacts with equal strength κ_0 with all neighbours within a range R_0 only, indicated by large magenta circles around selected oscillators. This is described by a finite range Kuramoto model. Oscillators can still affect one another over distances d larger than R_0, through chains of intermediary oscillators as sketched by the red lines without arrows.

forms the basis for the analytical part of our work. We then discuss how spatial correlation functions can be found in a series expansion in Sec. III, and validate our calculations through numerical simulations in Sec. IV. Section V explores if correlation functions in this model can be sampled based on an ergodicity assumption and Sec. VI shows how numerical simulations of the underlying model can constrain experimental parameters for the example of genetic oscillations in the segmentation clock. Details on the calculations in Sec. III are provided in Appendix A for lowest-order solutions and Appendix B for resummation to all orders. Appendix C presents a noise estimation method.

II. FINITE-INTERACTION-RANGE KURAMOTO MODEL

We consider a collection of N phase oscillators, arranged in either a square area of side length L in two dimensions, as sketched in Fig. 1, or a cubic box of side length L in three dimensions. Most results are presented for the two-dimensional (2D) case, for easier computations and visualization. Our general discussion applies to three dimensions as well. We assume the phase evolution of the oscillators is described by the set of coupled stochastic differential equations (SDEs)

$$d\theta_n(t) = \left[\omega_n - \sum_m^N \kappa_{nm} \sin(\theta_n - \theta_m)\right] dt + dW_n. \quad (1)$$

Here the index n labels each of the oscillators, which may differ in frequency ω_n and are located at specific, temporally fixed positions, $\boldsymbol{r}_n$. The random distribution of frequencies has a mean $\langle \omega_n \rangle = \overline{\omega}$ and a standard deviation $\Delta\omega$. For correlations of phases that we tackle later, the mean frequency $\overline{\omega}$ is irrelevant and hence can be set to zero without loss of generality. Here and in the following $\langle \cdots \rangle$ denotes the ensemble average. For this, quantities are averaged over a large set of solution to (1) with different noise realizations dW_n.

The coupling coefficients κ_{nm} are given by

$$\kappa_{nm} = \kappa_{\mathrm{nm}}(d) = \kappa_0 \theta(R_0 - |\boldsymbol{r}_n - \boldsymbol{r}_m|), \quad (2)$$

where θ is the Heaviside function, and thus κ_{nm} depend on the distance $d = |\boldsymbol{r}_n - \boldsymbol{r}_m|$ of two oscillators. The coupling acts with strength κ_0, only if oscillators are separated by at most R_0, and tends to synchronize phases owing to the sinusoidal dependence on the phase difference. Finally, each oscillator is subject to fluctuations randomizing the phases, dW_n, with correlations $\langle dW_n(t) dW_m(t') \rangle = 2\delta_{nm}\delta(t - t')/\beta$, where δ_{nm} is the Kronecker delta. Fluctuations are intrinsic to gene expression [30] but might also contain environmental contributions and in this model are controlled by the temperature type parameter β^{-1}. Mathematically, dW_n is the stochastic increment of a Wiener process [31]. The model (1) thus mainly differs from the original Kuramoto model by the introduction of a finite range R_0 of the coupling.

A special case of (1) is that of a homogenous frequency distribution, where all $\omega_n = \omega$ and hence $\Delta\omega = 0$. Counterintuitively, there are cases where this variant exhibits even more complicated dynamics than the heterogenous model, depending on the other ingredients, e.g., couplings κ_{nm} [32]. In this article we focus on the homogenous frequency model for tractable analytical calculations, and then show through direct simulations in the case of the heterogeneous frequency model to what extent our results are preserved in the latter.

Steady state in the homogenous frequency case

The set of Langevin equations (1) for $\omega_n = 0$ is equivalent to a Fokker-Planck equation (FPE) for the distribution function $p(\boldsymbol{\theta}, t)$ [31], where θ is the N-dimensional vector containing all phase angles $\boldsymbol{\theta} = [\theta_1, \ldots, \theta_N]^T$. Introducing the energy type expression

$$E = -\frac{1}{2}\mathbf{x}^\dagger K \mathbf{x}, \quad (3)$$

where $\boldsymbol{x} = [x_1, \ldots, x_N]^T$ with $x_n = \exp[i\theta_n]$ and K the coupling strength matrix with elements κ_{nm}, the FPE that corresponds to Eq. (1) can be written as [25,31]

$$\frac{dp(\boldsymbol{\theta}, t)}{dt} = -\sum_n \frac{\partial}{\partial\theta_n} F_n p(\boldsymbol{\theta}, t) + \sum_{nm} \frac{\partial^2}{\partial\theta_n \partial\theta_m} D_{nm} p(\boldsymbol{\theta}, t), \quad (4)$$

with drift coefficient $F_n = -\frac{\partial}{\partial\theta_n} E$ and diffusion coefficient $D_{nm} = \beta^{-1}\delta_{nm}$. The interpretation of the equivalence is that, if we propagate a stochastic ensemble of phases θ_n according to the noisy Kuramoto model (1), the function describing the random distribution of these phases will be $p(\boldsymbol{\theta}, t)$ and its evolution is given by Eq. (4).

An important property of the ensemble, that we utilize further below, is the degree of global synchronization encap-

sulated in the phase order parameter:

$$Z = \left| \sum_n x_n \right| / N. \tag{5}$$

We have $Z = 1$ when all oscillators lock into a synchronized phase, and $Z \to 0$ when phases are random. While it is not the main focus of our study, we usually indicate the synchronization level Z in the steady state for each choice of parameters later in the article.

It is now possible to analytically determine the steady-state distribution from Eq. (4) which fulfills $dp(\boldsymbol{\theta}, t)/dt = 0$, with the closed form solution [25]

$$p(\boldsymbol{\theta}) = \frac{1}{\mathcal{N}} \exp\left[-\beta E\right], \tag{6}$$

where $\mathcal{N} = \int d\theta^N \exp\left[-\beta E\right]$ is a normalization constant akin to a partition function. For the case $\Delta\omega = 0$ here, the steady-state distribution (6) of the FPE (4) evidently takes the form of a canonical equilibrium steady state. In contrast, for $\Delta\omega = 0$ the more complicated result would form a nonequilibrium steady state [33]. Based on Eq. (6), we now show how to calculate spatial correlation functions. Temporal autocorrelation functions are, for example, discussed in Ref. [33].

III. DISTANCE DEPENDENCE OF PHASE CORRELATIONS

As has been shown in Ref. [25], knowledge of the steady-state distribution (6) can be helpful to infer the coupling strengths κ_{nm} of an underlying model. They can be determined if *all* multioscillator correlations $\langle x_i^* x_j \rangle$ and $\langle x_i^* x_j^* x_k x_l \rangle$ in the steady state are known.

In practice, obtaining the information required, which includes all the averages $\langle x_i^* x_j \rangle$ and $\langle x_i^* x_j^* x_k x_l \rangle$, often poses a severe challenge: Obtaining convergence for fourth-order correlation functions will typically require a lot of reproducible repetitions of a given experiment. Also assigning fixed labels such as oscillator "n" versus oscillator "m" may be impossible if these numbers evolve in time or from realization to realization, because locations are not reproducible. Frequently even the total number within an ensemble may vary.

However, in many cases of interest, the detailed knowledge of all separate oscillator-oscillator couplings κ_{ij} is not required. When these are given by a simple distance-dependent formula such as Eq. (2), all that can be of interest are the parameters in the formula, in our case κ_0 and R_0. We show in the following that, assuming interactions (2), the distance dependence of ensemble averaged second-order correlations is sufficient to extract all model parameters for homogenous frequencies. We explicitly provide formulas for this in the regime where the coupling can be perturbatively dealt with. In the case of inhomogeneous frequencies, we show through simulations that a lot of information can still be obtained.

Inferring interaction strengths of a physical model from measured spatial correlation functions is a widely applied technique, for example, in elementary particle or condensed matter physics [34].

A. Series expansion

The clearest picture of the emergence of interoscillator correlations is obtained through a series expansion, where the coupling κ is assumed weak compared to the noise strength. Let us consider the pairwise phase correlation function

$$g_{ij} = \langle x_i x_j^* \rangle = \int d\theta^N x_i x_j^* p(\boldsymbol{\theta}, t) = \frac{\int d\theta^N x_i x_j^* e^{\frac{\beta}{2}\mathbf{x}^\dagger K \mathbf{x}}}{\int d\theta^N e^{\frac{\beta}{2}\mathbf{x}^\dagger K \mathbf{x}}}, \tag{7}$$

which we have now explicitly expressed through the underlying probability distribution (6). In the exponentials of Eq. (7), we now explicitly insert our interaction model (2) using $\kappa_{nm} = \kappa_0 \theta(R_0 - |\boldsymbol{r}_n - \boldsymbol{r}_m|)$, and obtain

$$\exp\left[\frac{\beta}{2}\mathbf{x}^\dagger K \mathbf{x}\right] = \exp\left[\frac{\beta\kappa_0}{2} \sum_{\substack{nm;n\neq m \\ |\boldsymbol{r}_n - \boldsymbol{r}_m| < R_0}} x_n x_m^*\right]. \tag{8}$$

We discuss in Appendix A how the integration over phases θ in Eq. (7) can be explicitly performed using a series expansion of the exponentials. The first few terms of that series may be sufficient if the parameter $\bar{\kappa} = \beta\kappa_0/2$ is small enough. Let us write

$$g_{ij} = \sum_{k=0}^{\infty} g_{ij}^{(k)}, \tag{9}$$

where $g_{ij}^{(k)} \sim \bar{\kappa}^k$ for the expansion of g_{ij} in powers of $\bar{\kappa}$.

We are only interested in correlations between different oscillators, for which $i \neq j$. Then $g_{ij}^{(0)} = 0$, expressing that two noninteracting oscillators are not correlated. The first-order term turns out nonzero, however, given by

$$g_{ij}^{(1)} = \frac{\beta\kappa_0}{2} \theta(R_0 - |\boldsymbol{r}_i - \boldsymbol{r}_j|), \tag{10}$$

hence only oscillators within each other's interaction range will be correlated and then exhibit a constant correlation strength. We thus notice that, if the leading order in perturbation theory is valid, a measurement of $g_{ij}^{(1)}$ already allows extraction of the range of interactions R_0 and the factor $\beta\kappa_0$. Using an independent way to determine the noise strength β^{-1}, which we discuss in Appendix C, also the coupling strength κ_0 can be determined.

It is instructive to also move to the second-order result, which is

$$g_{ij}^{(2)} = \left(\frac{\beta\kappa_0}{2}\right)^2 C_{ij;R_0}^{(1)}, \tag{11}$$

where $C_{ij;R_0}^{(k)}$ denotes the number of possible connections between oscillators i and j using (k) intermediate oscillators such that all links of the connection are shorter than R_0 (see Fig. 1). Hence the strength of correlations is set by $\beta\kappa_0$, while the spatial shape must depend on $C_{ij;R_0}^{(1)}$ (only). The derivation of all results above can be found in Appendix A.

We can generalize this intuitive concept to all higher orders in the perturbation expansion. For example, an interaction between oscillators i and j' in Fig. 1 arises in the eighth-order

term of the series expansion (9), as sketched by the longer red line.

For other applications of diagrammatic expansions as visualized in Fig. 1 to Kuramoto field theory, but with different variants of the model and aims, see, e.g., Ref. [35].

B. Summation to all orders

It turns out that, for some parameters, the series expansion underlying the previous section allows a complete resummation, enabling us to tackle also some nonperturbative conditions. As discussed in Appendix B we find

$$g_{ij} = \left[\frac{1}{1-\frac{\beta}{2}K}\right]_{ij}, \tag{12}$$

where K is the interaction matrix with elements κ_{ij}, the square brackets enclose a matrix function defined via the power series of $f(x) = 1/(1-\beta x/2)$, and subscripts ij then imply taking the corresponding matrix element of the result of the series.

Due to the finite radius of convergence of the series expansion of $f(x)$, Eq. (12) cannot be applied for all choices of parameters, but we demonstrate below that it reaches significantly further than the lowest orders (10) and (11).

IV. COMPARISON WITH SIMULATIONS

We now proceed to verify the expressions obtained so far through a direct numerical solution of the underlying stochastic equations (1). To this end, we first generated a set of N oscillator positions, uniform and randomly distributed in a square of side length L as sketched in Fig. 1. We chose a two-dimensional system for simplicity. Each oscillator also has a random initial phase $\theta_n(t=0) \in [0, 2\pi)$. For direct comparability with the analytical calculations above, we focus on the case of identical frequencies $\omega_n = \omega = 0$, unless otherwise indicated. We then calculate a solution of Eq. (1) using standard techniques within the high-level simulation package XMDS [36,37]. Simulation durations T are chosen such that the system had enough time to settle into its steady state.

We can determine phase-phase correlations such as Eq. (7) for each pair of oscillators from an ensemble average over $N_{\mathrm{traj}} = 640$ late time realizations of the simulation. These pairwise correlations are further averaged in bins, according to the spatial separation d between members of the pair, to obtain a simple one-dimensional correlation function $g(d)$. To be specific, we formally define

$$g(d) = \overline{g_{ij}}|_{d<|\boldsymbol{r}_i-\boldsymbol{r}_j|\leqslant d+\Delta d}, \tag{13}$$

with g_{ij} from Eq. (7). Here $\overline{\cdots}$ indicates the average over all pairs fulfilling the indicated constraint: their pair distance $|\boldsymbol{r}_i - \boldsymbol{r}_j|$ lies between d and $d+\Delta d$. Here Δd is a chosen discrete binning size. Throughout this section, we employ simple dimensionless units for all variables.

We show in Fig. 2 the resulting correlation functions for $N = 500$ oscillators within square boxes of side length $L = 1$, leading to a mean nearest-neighbor distance [38] of $\bar{d} = (2\sqrt{\rho})^{-1} \approx 0.02$ at density $\rho = N/L^2$. We implemented periodic boundary conditions over the box edges. The values at $d = 0$ are excluded from the figure since they contain g_{ii}, which are trivially equal to 1. To characterize the sample, we also indicate the ensemble averaged synchronization strength Z from Eq. (5) in each panel.

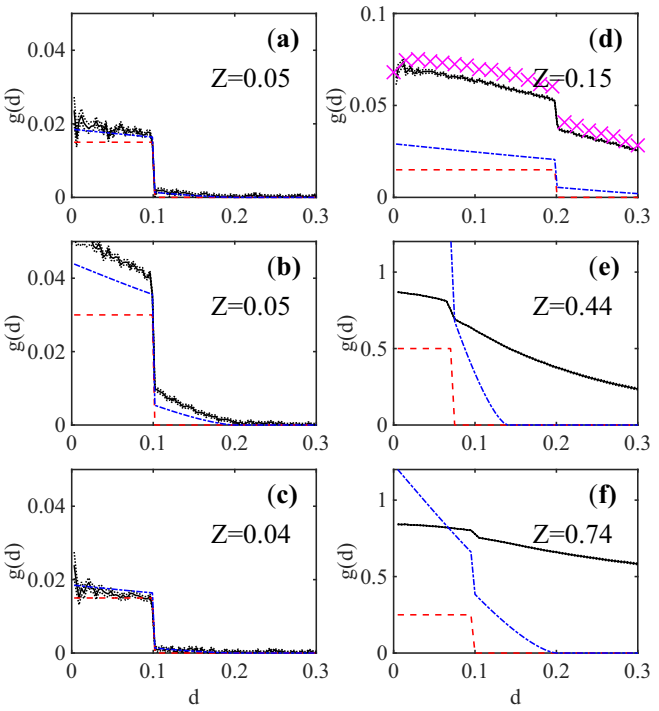

FIG. 2. Spatial phase-phase correlation functions $g(d)$ for $d > 0$ (solid black line). The standard error of the mean, Δg, is indicated by dotted lines at $g \pm \Delta g$. We compare with the analytical calculation of $g(d)$ from Sec. III A to leading order (red dashed) and second order (blue dot dashed). The synchronization Z from Eq. (5) is indicated in each panel. We compare different representative sets of parameters: (a) $\bar{\omega} = 0$, $\Delta\omega = 0$, $\kappa_0 = 0.03$, $R_0 = 0.1$, $\beta = 1$. (b) As (a), but with less noise, $\beta = 2$. (c) As (a), but with a distribution of frequencies $\Delta\omega = 0.5$. (d) As (a), but with longer-range interactions, $R_0 = 0.2$. Additionally, the resummed nonperturbative result (12) is shown as magenta (×); see text. (e) Strongly synchronized scenario with $\bar{\omega} = 0$, $\Delta\omega = 0.1$, $\kappa_0 = 0.2$, $R_0 = 0.07$, $\beta = 5$. (f) Using $\bar{\omega} = 0$, $\Delta\omega = 0.1$, $\kappa_0 = 0.05$, $R_0 = 0.1$, $\beta = 10$.

Most cases show a clear plateau with stronger correlations at short separations. This plateau now gives a good indication of the interaction range in the model, R_0, as for $d > R_0$ correlations almost drop to zero. Also the product of noise-parameter and interaction strength, $\alpha \sim \beta\kappa_0$, can be read from correlations, corresponding to the height of that plateau. Both observations are based on the derivations in Sec. III A. For Figs. 2(a) and 2(c), the lowest orders of the perturbation expansion almost quantitatively describe the correlations. However, in Fig. 2(d), despite a seemingly small perturbation parameter $\bar{\kappa} = 0.03$, deviations between simulation results and low-order perturbation theory arise. This highlights that the convergence of the series Eq. (9) with k not only depends on the smallness of the effective coupling, $\bar{\kappa}$, but also on the behavior of $C^{(k)}_{ij;R_0}$, which is the number of connections between the oscillators. The latter has significantly increased from Fig. 2(a) to Fig. 2(d), due to the doubled range of the potential. However, in this regime the resummed expression (12) gives good results, shown as magenta crosses.

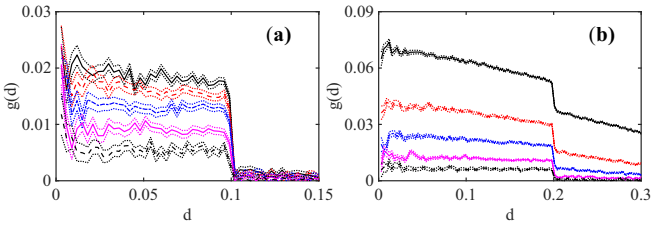

FIG. 3. Impact of frequency disorder on spatial phase correlation functions. (a) The same parameters as Fig. 2(c), except, from top to bottom, $\Delta\omega = 0$ (black solid line), $\Delta\omega = 0.5$ (red dashed line), $\Delta\omega = 1$ (blue dot dashed line), $\Delta\omega = 2$ (magenta solid line), and $\Delta\omega = 4$ (black dashed line). Dotted color matched lines indicate the stochastic sampling error as before. (b) The same parameters as in Fig. 2(d), with line styles as in (a).

For even more strongly synchronized scenarios than in Fig. 2(d), shown in Figs. 2(e) and 2(f), we find that the matrix series employed to evaluate Eq. (12) ceases to converge. While we empirically find that the precise range R_0 of the potential is still manifest in the correlation function as a clearly visible step, the difference between the plateau at $d < R_0$ and tail becomes less pronounced in this regime than in the perturbative or near-perturbative cases [Figs. 2(a)–2(d)].

We can also already see in Fig. 2(c) that our results are robust towards the addition of a moderate amount of frequency fluctuations $\Delta\omega$ among the oscillators, for which analytical calculations do not strictly apply. We explore this further in the following section. For the simulations in Fig. 2(c), we have assigned a random, temporally fixed frequency ω_n to each oscillator, prior to each stochastic solution of Eq. (1). These frequencies were drawn from the Gaussian distribution $p(\omega) = \exp[-\omega^2/(2[\Delta\omega]^2)]/(\sqrt{2\pi}\,\Delta\omega)$, with standard deviation $\Delta\omega$.

Inhomogeneous scenario with frequency spread

The objective of the previous section was to validate our analytical calculations in the clearly perturbative limit and then explore its limitations towards the nonperturbative regime. Another feature of model (1) that can limit the analytical results of Sec. III is a nonvanishing spread of oscillator frequencies $\Delta\omega$. While this can still be incorporated in the FPE (4) by redefining $E = -\frac{1}{2}\mathbf{x}^\dagger K\mathbf{x} + \sum_n \omega_n\theta_n$, we have not found a technique to evaluate correlation functions based on this expression. Nevertheless, the simulations in Fig. 2(c) already indicate that including weak frequency disorder $\Delta\omega$ does not fundamentally alter the results.

In Fig. 3 we show a more extensive simulation survey of the impact of frequency disorder $\Delta\omega$. We selected the cases from Fig. 2(c), with parameters that are safely in the perturbative regime, and Fig. 2(d), with parameters that require resummation to all orders in the calculation of correlation functions. For these cases we have successively increased the standard deviation $\Delta\omega$ of the Gaussian distribution of frequencies employed in the simulations.

It appears that the inclusion of random frequencies does not affect the spatial shape of the correlation function. Instead, increasing frequency disorder reduces the overall strength of correlations. This implies that measurements of correlation functions in these perturbative cases can still uniquely identify the range R_0 of interactions in Eq. (2).

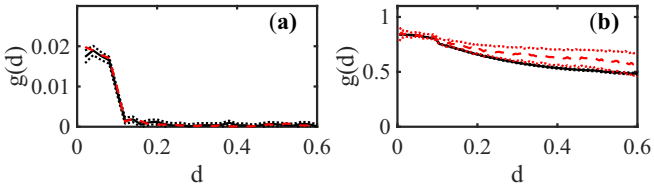

FIG. 4. Correlation function ergodicity. Black solid lines are correlation functions $g(d)$ obtained from the standard ensemble average, with black dashed lines indicating the sampling error. These are compared with $g(d)$ obtained from a time average within a single realization of the simulation, assuming ergodicity (red dashed). (a) Same parameters as Fig. 2(a). (b) Same parameters as Fig. 2(f).

V. CORRELATION ERGODICITY

For many experimental applications of model (1), a measurement related to an ensemble average may prove difficult. This in principle requires the repeated observation of identical systems, which may be impossible or require excessive experimental effort.

The problem can be circumvented if the physical system is ergodic, allowing us to replace the impossible ensemble average, such as $\langle x_i x_j^*\rangle$ with a long time average, such as $\overline{x_i x_j^*} \equiv \int_0^T x_i x_j^* dt/T$, for large T. While it may pose its own experimental challenges, this average is at least conceptually available.

In this section, we thus empirically determine whether the finite-range, homogenous Kuramoto model is ergodic regarding oscillator phase correlation functions. For this we consider full numerical solutions of Eq. (1) and compare ensemble averages over many realizations of Eq. (1), as discussed in Sec. IV, with long-time averages over a single realization. The results are shown in Fig. 4, for two selected cases already presented in Fig. 2.

While for the case of Fig. 4(a) it appears that ergodicity can be safely assumed, since the ensemble average and long-time average agree, for Fig. 4(b) this is only true for shorter distances. These results thus suggest caution and that further explorations are warranted.

VI. APPLICATION TO THE ZEBRAFISH SEGMENTATION CLOCK

We now consider phase correlation functions in a biophysical setting, as a practical illustration for the results presented here. Several systems in that field can be described by Kuramoto oscillators. We pick an example from the early vertebrate development, where the formation of the first muscular structures called "somites" is controlled by a molecular clock, the "segmentation clock." These somites give rise to veterbrae segments during later development of the embryo.

As an element of the clock, a population of autonomous cellular oscillators are coupled via delta-notch signaling, which results in oscillations of gene expression synchronized

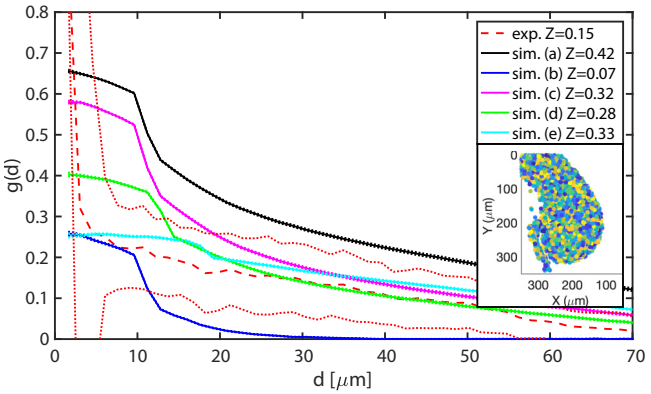

FIG. 5. Spatial phase correlation function from zebrafish embryo genetic oscillations compared with simulations of model (1). The experimental data described in the text are shown as a red dashed line, with statistical errors indicated by red dotted lines. We show only simulations where the parameters $\bar{\omega} = 0.15$ min^{-1}, $\Delta\omega = 0.07$ min^{-1} are matched to those extracted from Ref. [23]. In the following we list the varied parameters, where simulations are sorted in descending order of their correlation strength near $d \approx 0$: (a) $\kappa_0 = 0.55$ min^{-1}, $R_0 = 11$ μm, $\beta = 0.84$ min; (b) the same, but $\beta = 0.4$ min; (c) $\kappa_0 = 1.0$ min^{-1}, $R_0 = 11$ μm, $\beta = 0.4$ min; (d) $\kappa_0 = 0.5$ min^{-1}, $R_0 = 13$ μm, $\beta = 0.66$ min; and (e) $\kappa_0 = 0.18$ min^{-1}, $R_0 = 18$ μm, $\beta = 0.4$ min. Dashed color-matched lines indicate the sampling error, as before. The legend indicates the respective overall level of synchronization Z and the inset shows the initial spatial arrangement of cells in the experiment, for orientation.

between different cellular oscillators with a collective period [27]. As a result, a rhythmic wave of gene expression periodically traverses the embryonic presomitic mesoderm tissue [26], the arrest of which defines the boundaries of future segments of the organism.

One model for the formation of these waves is Eq. (1), where ω_i are cell intrinsic frequencies of genetic oscillation, κ_{ij} is intercellular coupling arising due to delta-notch signaling, and dW_n is the noise. Importantly, the precise dependence of the cell-cell coupling on distance, $\kappa_{\rm nm}(d)$, is unknown. While more complicated functional shapes $\kappa_{\rm nm}(d)$ could be studied in the future, we confine ourselves here to the finite-interaction-range Kuramoto-Sakaguchi model given by Eq. (2). Since the delta-notch interaction relies on cell-cell contacts, we would expect R_0 to be comparable in order of magnitude to the mean cell diameter, here roughly $d_{\rm cell} \approx 11$ μm.

The phases of individual cellular oscillators were experimentally determined from live embryos as described in Ref. [23]. The spatial distribution of the actual cellular oscillators is shown in the inset of Fig. 5. From the phases of individual oscillators, we then calculate the spatial phase correlations as in Eq. (7) but with the ensemble average replaced by a time average over the available experimental observation window (100 min). We thus invoke the assumption of ergodicity, explored in Sec. V. The result is shown in Fig. 5 as a red dashed line, with dotted lines indicating the standard error of the time average.

In this case, we find that no clear distinction between a plateau and a tail is possible within the experimental uncertainty, while the qualitative shape of the correlation function is reminiscent of those shown in Fig. 2. In order to demonstrate how information about the underlying interactions can still be obtained from the data, we compare the correlations with those from simulations of Eq. (1) for several selected parameter sets in Fig. 5. We show the ensemble averaged correlation function after the simulations have reached a steady state.

For simulations, we randomly distributed 800 oscillators (cells) within a cubic box of side length $L = 80$ μm, corresponding to a three-dimensional (3D) density $\rho_{\rm 3D} = 0.0014/\mu{\rm m}^3$, roughly matching the experiment, for which the more complicated actual cell distribution is shown in the inset of Fig. 5. We also adjusted the mean frequency to $\bar{\omega} = 0.15$ min^{-1} and their standard deviation to $\Delta\omega = 0.07$ min^{-1}, such that they correspond to the experimental values, averaged over the entire imaging region. Thus, importantly, these simulations correspond to the full-fledged Kuramoto model with inhomogeneous frequencies. Finally we estimated the noise content separately, using the technique proposed in Appendix C, and found $\beta = 0.4$ min. We thus mainly focus on the latter value in Fig. 5.

We find that, within model (2), interaction ranges R_0 slightly larger than the cell diameter $R_0 \approx 13$–18 μm can better reproduce the absence of a clearly visible plateau. Nonetheless, these values are reasonable based on the expectations from cell-cell contact interactions. Note that the shape of the correlation function is quite sensitive to R_0 for fixed κ and β, which both in turn do not affect the shape [see, e.g., Fig. 5, cases (a)–(c) in the legend].

After constraining the interaction range R_0 via the shape of the experimental correlation function, and the noise parameter β as in Appendix C, the best matching coupling strengths based on this demonstration are roughly $\kappa_0 \approx 0.18$ min^{-1}. It is tempting to compare this value with those from existing parameter extractions in Refs. [27,28,39], which report $\kappa_0 = \epsilon/N_n$, with $\epsilon = 0.07$ min^{-1} where N_n is the number of cell neighbors and a noise given by $\beta = 154$ min [translated to the noise term used here in Eq. (1)]. However, note that the models underlying the parameter extraction in Refs. [27,28,39] exclusively assume a *two-dimensional* arrangement of oscillators. The corresponding qualitative change in connectivity can explain, for example, the significantly different noise parameter to reach similar synchronization strengths, as previous work has shown that the oscillator network topology significantly influences synchronization [40]. It is encouraging, though, that the order of magnitude for the coupling inferred here is in rough agreement with earlier results, despite the vastly different approaches.

We also analyzed the data for oscillators in the posterior only, excluding the anterior which shows quite different synchronization behavior [23]. This gave very similar results.

Note that a few important features of the *in vivo* system are ignored here: time delays [28], wave propagation, synchronization oscillations [23], and cellular motion [24,29,41]. This would be justified if correlations behave ergodically despite these complications, and clearly a study of correlation functions including these aspects would be desirable, but is deferred to future work. Motion could for example effectively increase the range of interactions [41] and thus contribute

to the extracted R_0 here being slightly larger than the cell radius.

VII. CONCLUSIONS AND OUTLOOK

We have analytically and numerically studied phase-phase correlation functions in a finite-range Kuramoto model. The model is for example used to describe cellular gene expression oscillations involved in the segmentation clock regulating the growth of somites in developing zebrafish embryos.

Using a perturbation expansion, we develop analytical expressions for phase correlations under weakly and intermediately synchronized conditions for the case of identical oscillator frequencies. These are verified with numerical simulations. In the weakly synchronized case, we show that the interaction potential strength and range can be directly inferred from the correlation data, provided the strength of noise sources in the system is known. We also propose a method by which the latter can be approximately inferred independently. Our simulations show that analytical results are qualitatively applicable to models with a spread of frequencies as well.

We finally compare the numerical model with experimental data to demonstrate the extent to which interaction parameters can be constrained by correlations. Important aspects of the real biophysical system that require extensions of the present work are the inclusion of time delays [28], motion of cells or oscillators [24], and thus changing connectivity [42] as well as traveling gene expression waves [43–45].

Another important feature of realistic settings to which the present analytical calculations should be extended is a nonvanishing distribution of frequencies, maybe following techniques similar to those in Ref. [46].

ACKNOWLEDGMENTS

We thank Saùl Ares and Shamik Gupta for helpful comments on the manuscript. S.W. is grateful for financial support from the Max Planck Society under the MPG-IISER partner group program.

APPENDIX A: LOW-ORDER CORRELATION FUNCTIONS

As discussed in Sec. III A, we can explicitly evaluate Kuramoto model correlation functions using

$$g_{ij} = \frac{\int d\theta^N x_i x_j^* e^{\frac{\beta}{2}\mathbf{x}^\dagger K \mathbf{x}}}{\int d\theta^N e^{\frac{\beta}{2}\mathbf{x}^\dagger K \mathbf{x}}}. \tag{A1}$$

First, expanding the exponential function in the numerator, we obtain

$$\begin{aligned} g_{ij} &= \mathcal{N}^{-1} \int d\theta^N x_i x_j^* \exp\left[\frac{\beta\kappa_0}{2} \sum_{\substack{nm;n\neq m \\ |\boldsymbol{r}_n - \boldsymbol{r}_m|<R_0}} x_n x_m^*\right] \\ &= \mathcal{N}^{-1} \int d\theta^N x_i x_j^* \Bigg[1 + \frac{\beta\kappa_0}{2} \sum_{\substack{nm;n\neq m \\ |\boldsymbol{r}_n - \boldsymbol{r}_m|<R_0}} x_n x_m^* \\ &\quad + \frac{1}{2}\left(\frac{\beta\kappa_0}{2}\right)^2 \sum_{\substack{nm;n\neq m \\ |\boldsymbol{r}_n - \boldsymbol{r}_m|<R_0}} x_n x_m^* \sum_{\substack{kl;k\neq l \\ |\boldsymbol{r}_k - \boldsymbol{r}_l|<R_0}} x_k x_l^* \\ &\quad + O\left(\frac{\beta\kappa_0}{2}\right)^3\Bigg]. \end{aligned} \tag{A2}$$

This expansion will typically be useful if $\alpha = \beta\kappa_0/2 \ll 1$, but only if the coefficients of the powers of α^k do not increase too rapidly with k. The former condition will be fulfilled if the coupling strength κ_0 is much less than the noise strength β^{-1}.

We are only interested in correlations between different oscillators; hence, let us set $i \neq j$. In that case the zero-order term in $(\beta\kappa_0)$ vanishes, since $\int_0^{2\pi} d\theta\, x_k = \int_0^{2\pi} d\theta \exp[i\theta_k] = 0$. In general, for the same reason, any term in Eq. (A2) will vanish, unless all complex exponential functions contained within are combined into pairs with identical indices and one conjugate, such as $(x_i x_{m=i}^*)$. We then find for the first-order term (up to $k = 1$)

$$\begin{aligned} g_{ij}^{(1)} &\equiv \frac{\beta\kappa_0}{2\mathcal{N}} \int d\theta^N \sum_{\substack{nm;n\neq m \\ |\boldsymbol{r}_n - \boldsymbol{r}_m|<R_0}} x_i x_j^* x_n x_m^* \\ &= \frac{\beta\kappa_0}{2\mathcal{N}} \int d\theta^N \sum_{\substack{nm;n\neq m \\ |\boldsymbol{r}_n - \boldsymbol{r}_m|<R_0}} \delta_{im}\delta_{jn} \\ &= \frac{\beta\kappa_0}{2\mathcal{N}} (2\pi)^N \theta(R_0 - |\boldsymbol{r}_i - \boldsymbol{r}_j|). \end{aligned} \tag{A3}$$

In the last equality, we have used that the double sum only contains indices $m = i$ and $n = j$, if oscillator i and j are separated by less than the interaction range R_0.

For the final evaluation we require the normalization factor $\mathcal{N}$, which can similarly be obtained as a power series in α, using

$$\begin{aligned} \mathcal{N} &= \int d\theta^N \left[\frac{\beta\kappa_0}{2} \sum_{\substack{nm;n\neq m \\ |\boldsymbol{r}_n - \boldsymbol{r}_m|<R_0}} x_n x_m^*\right] \\ &= \int d\theta^N \left[1 + \frac{\beta\kappa_0}{2} \sum_{\substack{nm;n\neq m \\ |\boldsymbol{r}_n - \boldsymbol{r}_m|<R_0}} x_n x_m^* + O\left(\frac{\beta\kappa_0}{2}\right)^2\right]. \end{aligned} \tag{A4}$$

Since Eq. (A3) already contains one power of $\beta\kappa_0$, to obtain the leading nonvanishing contribution, we can use a normalization factor $\mathcal{N} = (2\pi)^N$, which is valid to zero and first order. Altogether we obtain as the first nontrivial contribution to the correlation function

$$g_{ij}^{(1)} = \frac{\beta\kappa_0}{2}\theta(R_0 - |\boldsymbol{r}_i - \boldsymbol{r}_j|), \tag{A5}$$

shown and discussed in Sec. III A.

It is instructive to proceed to the second-order term in the perturbation expansion, which introduces longer-range correlations through the effect of intermediary oscillators. From Eq. (A2), we have

$$g_{ij}^{(2)} \equiv \frac{\alpha^2}{\mathcal{N}} \int d\theta^N x_i x_j^* \sum_{\substack{nm;n\neq m \\ |\boldsymbol{r}_n - \boldsymbol{r}_m|<R_0}} x_n x_m^* \sum_{\substack{kl;k\neq l \\ |\boldsymbol{r}_k - \boldsymbol{r}_l|<R_0}} x_k x_l^*. \tag{A6}$$

The same arguments that led to our first-order expression allow us to identify this as the sum over all possible connections from oscillator i to oscillator j using one intermediary oscillator, as sketched with two red lines in the bottom left part of Fig. 1. The region in which these intermediary oscillators can be located, given the interaction range constraints, is shaded in blue.

We can thus write

$$g_{ij}^{(2)} = \frac{\alpha^2}{\mathcal{N}}(2\pi)^N C_{ij;R_0}^{(1)}, \tag{A7}$$

where $C_{ij;R_0}^{(k)}$ denotes the number of possible connections between oscillators i and j using (k) intermediate oscillators such that all links of the connection are shorter than R_0.

Assuming a large number density of oscillators ρ, we can estimate $C_{ij;R_0}^{(1)}$ as $C_{ij;R_0}^{(1)} = \rho A(\boldsymbol{r}_i, \boldsymbol{r}_j, R_0)$, where in our 2D case A is the overlap area of two circles with radii R_0 that are centered on the oscillator positions $\boldsymbol{r}_i$ and $\boldsymbol{r}_j$, which are separated by a distance d. This corresponds to the blue shaded area in Fig. 1. Using

$$A(\boldsymbol{r}_i, \boldsymbol{r}_j, R_0) = 2R_0^2 \cos^{-1}\left(\frac{d}{2R_0}\right) - \frac{\sqrt{(2R_0 - d)d^2(2R_0 + d)}}{2}, \tag{A8}$$

where this is real and positive, and $A = 0$ otherwise, we can write

$$g_{ij}^{(2)}(d) = \rho\alpha^2 A(\boldsymbol{r}_i, \boldsymbol{r}_j, R_0). \tag{A9}$$

We could generalize this intuitive concept to all higher orders in the perturbation expansion. For example, an interaction between oscillators i and j' in Fig. 1 arises in eighth-order perturbation theory, as sketched by the longer red line. However, we have not succeeded to analytically evaluate quantities like $C_{ij;R_0}^{(8)}$ that would be required in that case.

APPENDIX B: EVALUATION TO ALL ORDERS

It is, however, possible to evaluate the series in Eq. (9) to all orders, in a brute force approach. To this end, let us first inspect the role of the normalization factor $\mathcal{N}$ in the calculation of g_{ij} more closely. Note that the numerator and denominator in Eq. (A1) are very similarly structured, except that there are no "external" phase factors x_i, x_j in the expression for $\mathcal{N}$.

Consequently, applying the diagrammatic reasoning discussed in the previous section, the normalization factor in the denominator quantifies the contribution of "closed loop" diagrams as shown in Fig. 6 at the bottom. For example the left-most triangular loop would correspond to a contribution

$$\sim \int d\theta^N x_a x_b^* x_b x_c^* x_c x_a^* \tag{B1}$$

to the integration in Eq. (A4), where a, b, and c are the indices of oscillators involved in the triangle. Note, however, that these closed loop diagrams would also contribute to the numerator as diagrammatically shown in Fig. 6. The effect of the denominator, to any given order in α, is thus to precisely cancel the contribution to our series expansion of all chains of connected oscillators in which the two target sites of interest, i and j, are not directly connected. The precisely same mathematical features arise in diagrammatic expansions of quantum field theory, where the normalization factor is known to reduce the set of all Feynman diagrams to the set of "connected diagrams," by canceling "vacuum diagrams" [34].

Using this constraint allows a simplified evaluation of the integrals in Eq. (A1) to all orders: Let us write

$$g_{ij} = \frac{1}{(2\pi)^N}\int d\theta^N x_i x_j^* e^{\frac{\beta}{2}\mathbf{x}^\dagger K \mathbf{x}}\Big|_{\text{connected}}, \tag{B2}$$

implying that in the series expansion the terms x_i and x_j^* are to be joined by one connected list of additional phase factors as exemplified to second order in Eq. (A6) and Fig. 1. We also incorporated that the leading order of $\mathcal{N}$ is $(2\pi)^N$; see Appendix A.

When expanding the exponential

$$\begin{aligned} g_{ij} &= \frac{1}{(2\pi)^N}\int d\theta^N x_i x_j^* \sum_k \frac{(\beta/2)^k}{k!} \\ &\quad \times \sum_{n_1,m_1}\cdots\sum_{n_k,m_k}[x_{n_1}^*\kappa_{n_1m_1}x_{m_1}]\cdots[x_{n_k}^*\kappa_{n_1m_1}x_{m_k}]\Big|_{\text{connected}} \\ &= \frac{1}{(2\pi)^N}\int d\theta^N \sum_k \frac{(\beta/2)^k}{k!}k! \\ &\quad \times \sum_{n_1,m_1}\cdots\sum_{n_k,m_k}\underbrace{x_i[x_{n_1}^*}_{=\delta_{in_1}}\kappa_{n_1m_1}\underbrace{x_{m_1}]x_{n2}^*}_{=\delta_{m_1n_2}}\cdots\underbrace{x_{m_{k-1}}[x_{n_k}^*}_{=\delta_{m_{k-1}n_k}}\kappa_{n_1m_1}\underbrace{x_{m_k}]x_j^*}_{=\delta_{m_kn_j}}. \end{aligned} \tag{B3}$$

In the second equality we have written the requirement that two adjacent phase factors must have identical indices in order to yield a nonzero integral. Note the following:

(i) There are $k!$ permutations of intermediary phase factors such that they overall connect x_i and x_j^*; hence we have added a factor $k!$.

(ii) With the connections implied by $\underbrace{\cdots}$, x_i and x_j must be connected to each other and all other x_n terms, hence we dropped the tag "connected."

We can now exploit the Kronecker deltas and perform the final trivial integration over $d\theta^N$ to arrive, after renaming indices, at

$$\begin{aligned} g_{ij} &= \sum_k (\beta/2)^k \sum_{m_1,m_{k-1}} \kappa_{n_im_1}\kappa_{m_1m_2}\cdots\kappa_{m_{k-2}m_{k-1}}\kappa_{m_{k-1}n_j} \\ &= \sum_k (\beta/2)^k [K^k]_{ij}. \end{aligned} \tag{B4}$$

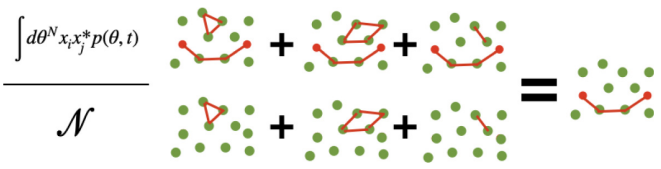

FIG. 6. Cancellation of disconnected elements of diagrams in the series expansion of correlations. The top row indicates some selected contributions to the numerator with target sites ij marked as red dots. In addition to one identical connection via two intermediate oscillators, additional closed loops may appear. Only the closed loops also appear in the numerator. In a rigorous order-by-order expansion of both, the numerator thus cancels all disconnected elements.

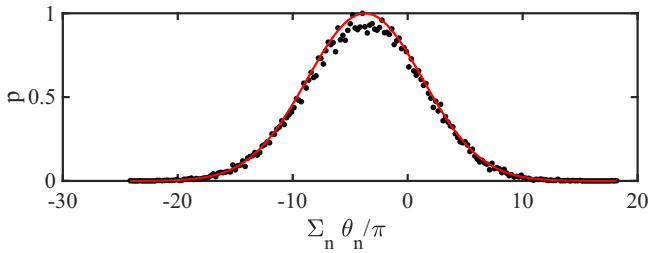

FIG. 7. Extraction of noise amplitude in model (1) through sampling of the time-increment histogram. Black (•): histogram of phase increments $\Delta\Theta$ for 240 000 time samples of length $\Delta t = 2.5$ for the same parameters as in Fig. 2(f). The red line is the theoretical expectation as described in the text.

We have recognized the summations as the k-fold matrix power of K; the symbol $[]_{ij}$ implies taking matrix elements ij. Finally using the series expansion $1/(1-x) = \sum_{k=0}^{\infty} x^k$ for $|x| < 1$, applied to a series of matrices, we arrive at Eq. (12).

The agreement between the result based on the discussion of this section and a complete simulation in Fig. 2(d) ultimately validates the approach above, regarding a cancellation of disconnected elements of the diagrams. Unfortunately the finite radius of convergence of the series expansion employed apparently limits its use to an intermediate range of degrees of synchronization.

APPENDIX C: NOISE AMPLITUDE DETERMINATION

As described in Sec. III, an extraction of the interaction parameters of interest from the spatial dependence of phase correlations is only possible if we have a separate means to determine the noise-strength parameter β^{-1}. One way to obtain information about the noise is to consider the sum of all oscillator phases $\Theta = \sum_n \theta_n$. Using model (1), we find that the time evolution of summed phases is given by

$$d\Theta(t) = \sum_n^N \omega_n dt + \sum_n^N dW_n = \Omega\, dt + d\xi. \tag{C1}$$

The interactions have dropped out of the equation due to their antisymmetry $\kappa_{nm} \sin(\theta_n - \theta_m) = -\kappa_{mn} \sin(\theta_m - \theta_n)$. In the second equality we have defined a summed frequency $\Omega = \sum_n^N \omega_n$ and summed noise term $d\xi = \sum_n^N dW_n$. As the sum of the N Gaussian random processes dW_n, the variable $d\xi$ is simply another random Gaussian process with variance $2N/\beta$.

By integrating Eq. (C1) over a short time interval Δt, one can then show that increments in time $\Delta\Theta = \Theta(t + \Delta t) - \Theta(t)$ are again Gaussian distributed, with mean $\Omega\Delta t$ and variance $2N\Delta t/\beta$. When $\Theta(t)$ can be experimentally extracted for sufficiently many time samples, the variance of the increments thus allows us to infer β.

Exemplarily, this is demonstrated in Fig. 7, where we show a histogram of increments between different time samples of Eq. (C1), obtained from the simulation in Fig. 2(f), clearly showing the Gaussian statistics. We would infer $\beta = 10.003$ from these noisy data, with a simulation parameter of $\beta = 10$.

[1] Y. Kuramoto, in *Lecture Notes in Physics Vol. 30*, edited by H. Araki (Springer, New York, 1975), p. 420.
[2] Y. Kuramoto, *Chemical Oscillations, Waves, and Turbulence* (Springer, Berlin, 1984).
[3] J. A. Acebrón, L. L. Bonilla, C. J. Pérez Vicente, F. Ritort, and R. Spigler, Rev. Mod. Phys. **77**, 137 (2005).
[4] S. H. Strogatz, *Sync: How Order Emerges from Chaos in the Universe, Nature, and Daily Life* (Penguin, New York, 2012).
[5] E. Montbrió and D. Pazó, Phys. Rev. Lett. **120**, 244101 (2018).
[6] V. Flovik, F. Macià, and E. Wahlström, Sci. Rep. **6**, 32528 (2016).
[7] K. Wiesenfeld, P. Colet, and S. H. Strogatz, Phys. Rev. Lett. **76**, 404 (1996).
[8] B. R. Trees, V. Saranathan, and D. Stroud, Phys. Rev. E **71**, 016215 (2005).
[9] J. Javaloyes, M. Perrin, and A. Politi, Phys. Rev. E **78**, 011108 (2008).
[10] J. Buck and E. Buck, Sci. Am. **234**, 74 (1976).
[11] L. Wolpert, J. Smith, T. Jessell, P. Lawrence, E. Robertson, and E. Meyerowitz, *Principles of Development* (Oxford University Press, Oxford, 2016).
[12] J. Lewis, Curr. Biol. **13**, 1398 (2003).
[13] I. Palmeirim, D. Henrique, D. Ish-Horowicz, and O. Pourquie, Cell **91**, 639 (1997).
[14] M. Kaern, M. Menziger, and A. Hunding, J. Theor. Biol. **207**, 473 (2000).
[15] A. Pikovsky, M. Rosenblum, and J. Kurths, *Synchronization: A Universal Concept in Nonlinear Sciences* (Cambridge University Press, Cambridge, UK, 2001).
[16] S. Gupta, A. Campa, and S. Ruffo, J. Stat. Mech.: Theory Exp. 08 (2014) R08001.
[17] H. Hong, H. Park, and M. Y. Choi, Phys. Rev. E **72**, 036217 (2005).
[18] S.-Y. Ha, Z. Li, and X. Xue, J. Diff. Equations **255**, 3053 (2013).
[19] H. Schuster and P. Wagner, Prog. Theor. Phys. **81**, 939 (1989).
[20] B. C. Bag, K. G. Petrosyan, and C.-K. Hu, Phys. Rev. E **76**, 056210 (2007).
[21] H. Sakaguchi, Prog. Theor. Phys. **79**, 39 (1987).
[22] R. Bhavna, K. Uriu, G. Valentin, J. Tinevez, and A. Oates, PLoS One **11**, e0161550 (2016).
[23] R. Bhavna, Dev. Biol. **460**, 55 (2020).
[24] K. Uriu, R. Bhavna, A. C. Oates, and L. G. Morelli, Biol. Open **6**, 1235 (2017).
[25] C. F. Cadieu and K. Koepsell, Neural Comput. **22**, 3107 (2010).
[26] A. C. Oates, L. G. Morelli, and S. Ares, Development (Cambridge, U.K.) **139**, 625 (2012).
[27] L. Herrgen, S. Ares, L. G. Morelli, C. Schröter, F. Jülicher, and A. C. Oates, Curr. Biol. **20**, 1244 (2010).

[28] L. G. Morelli, S. Ares, L. Herrgen, C. Schröter, F. Jülicher, and A. C. Oates, HFSP J. **3**, 55 (2009).
[29] K. Uriu and L. Morelli, Biophys. J. **107**, 514 (2014).
[30] A. Raj and A. van Oudenaarden, Cell **135**, 216 (2008).
[31] C. W. Gardiner, *Handbook of Stochastic Methods* (Springer-Verlag, Berlin, 2003).
[32] H. Hong and S. H. Strogatz, Phys. Rev. E **84**, 046202 (2011).
[33] D. Das and S. Gupta, J. Phys. A: Math. Theor. **51**, 445003 (2018).
[34] M. E. Peskin and D. V. Schroeder, *An Introduction to Quantum Field Theory* (Perseus, New York, 1995).
[35] M. A. Buice and C. C. Chow, Phys. Rev. E **76**, 031118 (2007).
[36] G. R. Dennis, J. J. Hope, and M. T. Johnsson, Comput. Phys. Commun. **184**, 201 (2013).
[37] G. R. Dennis, J. J. Hope, and M. T. Johnsson (2012), http://www.xmds.org/
[38] P. Hertz, Math. Ann. **67**, 387 (1909).
[39] I. H. Riedel-Kruse, C. Müller, and A. C. Oates, Science **317**, 1911 (2007).
[40] F. A. Rodrigues, T. K. D. Peron, P. Ji, and J. Kurths, Phys. Rep. **610**, 1 (2016).
[41] K. Uriu, S. Ares, A. C. Oates, and L. G. Morelli, Phys. Rev. E **87**, 032911 (2013).
[42] A. Banerjee and M. Acharyya, Phys. Rev. E **94**, 022213 (2016).
[43] D. Iatsenko, S. Petkoski, P. V. E. McClintock, and A. Stefanovska, Phys. Rev. Lett. **110**, 064101 (2013).
[44] C. R. Laing, Chaos **26**, 094802 (2016).
[45] O. E. Omel'chenko, M. Wolfrum, and C. R. Laing, Chaos **24**, 023102 (2014).
[46] N. Uchida, Phys. Rev. Lett. **106**, 064101 (2011).